Haloplumbate Nanochains Templated by Quaternary Phosphorus: Good Water Stabilities, Thermochromic Luminescence and Photocurrent Responses①

CUI Jian-Hao[a] ZHANG Wen-Ting[b]
ZHENG Hui-Dong[a, c②] LI Hao-Hong[b, c②]
[a] (*College of Chemical Engineering, Fuzhou University, Fuzhou* 350108, *China*)
[b] (*College of Chemistry, Fuzhou University, Fuzhou* 350108, *China*)
[c] (*Fujian Engineering Research Center of Advanced Manufacturing Technology for Fine Chemicals, Fuzhou University, Fuzhou* 350108, *China*)

ABSTRACT Two triphenylmethylphosphonium/haloplumbate hybrids, *i.e.*, $[(PPh_3Me)_2(Pb_2I_6)\cdot CH_3CN]_n$ (**1**) and $[(PPh_3Me)(PbBr_3)]_n$ (**2**), have been prepared, in which the $(PbX_3)_n^{n-}$ nanochains built from face-sharing PbX_6 octahedra are surrounded by organic templates to assemble the core-shell quantum well. Besides, C−H $\cdots\pi$ interactions among Ph_3PMe^+ cations can also be detected, which give rise to the 2-*D* organic layer of **1** and 1-*D* chain for **2**. The good water stabilities could be induced by the strong C−H $\cdots\pi$ interactions, which can deter the hydrolysis reaction. The energy band gaps of this work mainly derive from the charge transfer of organic components, but their luminescence stems from the inorganic $(PbX_3)_n^{n-}$ nanochains with co-existence of free excitons and self-trapped excitons. At temperature lower than 117 K, strong quantum confinement will rule out the free excitons, and self-trapped excitons will dominate, resulting in red-shift luminescence. Moreover, effective and repeatable photocurrent responses can be found in these hybrids.

Keywords: organic-inorganic hybrid, haloplumbate, quaternary phosphorus, photoluminescence, photocurrent response; DOI: 10.14102/j.cnki.0254–5861.2011–3009

1 INTRODUCTION

Inorganic-organic hybrids have emerged as new-generation optoelectronic functional materials with fascinating structures and regulatable properties for a variety of applications[1], for example, photovoltaics[2], light-emitting devices[3], photo/thermochromism[4, 5], photocatalytic degradation[6] and photo/X-ray detectors[7]. Among them, lead(II) halide-based ones have attracted special attention owing to its large radius, flexible coordination environment, and variable stereochemical activities of lead center[8]. So far, haloplumbates with structural dimensions range from zero-dimensional (0-*D*) to three-dimensional (3-*D*) by means of vertex-, edge-, or face-sharing PbX_6 octahedra have been explored extensively[9]. Recently, special attention was paid to the 1-*D* nanochain haloplumbate-based hybrids on their gap engineering, luminescence and conductivity[10]. For example, the 1-*D* haloplumbate hybrids showed white-light-emitting with high quantum efficiency[11]. Moreover, the 1-*D* metal halide chains associated with π-packing organic components showed synergistic conductance, even metallic behavior[12]. Therefore, the haloplumbates with 1-*D* nanochains are still significant for new opt/electrical materials, and there is still big space in structure/property modulation by introducing various organic functional templates[1]. And the interactions between the extended inorganic chains and organic components can be carefully adjusted by manipulating the metals, halides, and organic components.

Triphenylphosphonium derivates are good candidates as structural templates, because they possess three phenyl groups and one other substituent, which can be used as organic long-persistent luminescent materials[13]. Besides, the alkyl group can deter the dispersing of organic and inorganic moieties, thus enhancing their water stabilities[14]. So far, the

Received 26 January 2020; accepted 28 February 2020 (**CCDC 1590157 for 1 and 1874784 for 2**)
① This work was financially supported by the National Natural Science Foundation of China (No. 22078065)
② Corresponding authors. E-mails: youngman@fzu.edu.cn and lihh@fzu.edu.cn

quaternary phosphorus was seldom utilized as templates in haloplumbate system, which might be due to its more difficulty in structural modification. To our knowledge, only limited haloplumbates/quaternary phosphorus hybrids were reported. Furthermore, the property investigation was still in its infancy[15-19]. In this work, triphenylmethylphosphonium was used as template to synthesize two new haloplumbate hybrids, *i.e.*, $[(PPh_3Me)_2(Pb_2I_6)\cdot CH_3CN]_n$ (**1**) and $[(PPh_3Me)(PbBr_3)]_n$ (**2**). They exhibit red emissions with good water stability. In addition, excellent photocurrent responses can be detected.

2 EXPERIMENTAL

2. 1 Materials and methods

All chemicals except quaternary phosphorus $(PPh_3Me)\cdot I$ were commercial products and used without further purification. IR spectra were recorded on a Perkin-Elmer Spectrum-2000 FTIR spectrophotometer (4000～2400 cm^{-1}) on powdered sample spread on KBr plate. Elemental analyses for C, H and N were performed on a Vario MICRO elemental analyzer. Optical diffuse reflectance spectra were measured on a Perkin-Elmer lambda 900 UV/VIS spectrophotometer equipped with an integrating sphere at 293 K, and $BaSO_4$ plates were used as reference. Powder XRD patterns were obtained using a Philips X'Pert-MPD diffractometer with Cu$K\alpha$ radiation (λ = 1.54056 Å). Fluorescence spectra were carried out on an Edinburgh FL-FS 920 TCSPC spectrometer. The luminescence quantum yields were recorded on a Hamamatsu Photonics C11347-11 absolute photoluminescence quantum yield spectrometer. ^{1}H NMR spectra were recorded on a Bruker Advance III 400 MHz NMR spectrometer. The photocurrent experiments were performed on a CHI650 electrochemistry workstation with three-electrode systems.

2. 2 Synthesis

2. 2. 1 Synthesis of $(PPh_3Me)\cdot I$

$(PPh_3Me)\cdot I$ was synthesized by one step alkylated reaction of triphenylphosphine with iodomethane in the toluene solvent according to literature method[20]. CH_3I (0.0930 g, 0.66 mmol) was slowly added into a chilled solution of 0.48 mmol Ph_3P (0.1261 g) in 10 mL of toluene, which was reacted in a 100 mL round-bottomed flask in an ice bath. The mixed solution was stirred for 1 h at 0 ℃, and the solvent was removed by rotation volatilization at 80 ℃. The residue was washed with fresh toluene and dried in the oven. White powder (Ph_3PCH_3I) was obtained with more than 98% yield. ^{1}H NMR (400 MHz, Chloroform-*d*): δ 7.86～7.61 (m, 11H), 7.33 (s, 4H), 3.25 (dd, *J* = 13.2, 3.7 Hz, 3H).

2. 2. 2 Synthesis of $[(PPh_3Me)_2(Pb_2I_6)\cdot CH_3CN]_n$ (1)

1 was prepared by solution evaporation method. PPh_3MeI (0.0808 g, 0.2 mmol) and PbI_2 (0.0380 g, 0.2 mmol) were dissolved in 20 mL acetonitrile, and kept stirring at 45 ℃ for 2 hours. The obtained solution was filtered, and yellow filtrate liquor was covered with a cling film at room temperature for slow evaporation. Yellow block crystals were obtained after 30 minutes. Yield: 85.1% (0.0621 g, based on Pb). Anal. Calcd. for $C_{40}H_{39}I_6NP_2Pb_2$ (1771.53): C, 27.12; H, 2.22; N, 0.79%. Found: C, 27.35; H, 2.15; N, 1.03%. IR (cm^{-1}): 3079(w), 2980(w), 1594(m), 1498(s), 1372(w), 1090(s), 814(w), 771(s), 726(s), 694(s), 490(s), 448(w).

2. 2. 3 Synthesis of $[(PPh_3Me)(PbBr_3)]_n$ (2)

The synthesis process is similar to that of **1**, expect that $(PPh_3Me)Br$ (0.1546 g, 0.383 mmol) and $PbBr_2$ (0.045 g, 0.192 mmol) were used as starting materials and methanol as solvent. Colorless block crystals were obtained after 30 minutes. Yield: 63.1% (0.1042 g, based on Pb). Anal. Calcd. for $C_{19}H_{18}Br_3PPb$ (724.20): C, 31.51; H, 2.50%. Found: C, 31.36; H, 2.72%. IR (cm^{-1}): 3050(w), 2977(w), 1584(w), 1480(w), 1452(m), 1315(w), 1116(m), 888(m), 752(s), 679(s), 484(s).

2. 3 Electrode preparation and photocurrent measurement

Typical solution coating method is utilized to prepare the photocurrent measurement electrodes of **1** and **2**[21, 22]. 5 mg as-synthesized powder was dissolved in 0.3 mL DMF, and the suspension was dispersed evenly to obtain slurry which was spread onto the pre-cleaned ITO glass (0.6 × 0.6 cm^2, 14 $\Omega\cdot per\cdot cm^2$) with its side part previously protected using scotch tape. The working electrode was dried overnight under ambient conditions. A copper wire was connected to the side part of the working electrode using a conductive tape. Uncoated parts of the electrode were isolated with epoxy resin. A 150 W high-pressure xenon lamp, located 15 cm away from the surface of the ITO electrode, was employed as a full-wavelength light source. The photocurrent experiments were performed on a CHI660 electrochemistry workstation in a three-electrode system, with the sample-coated ITO glass as the working electrode mounted on the window with an area of 0.25 cm^2, a Pt wire as the auxiliary electrode, and a Ag/AgCl electrode as the reference electrode. The supporting electrolyte solution was a 0.2 mol L^{-1} sodium sulfate aqueous

solution. The applied potential was 0.5 V for all measurements. The lamp was kept on continuously, and a manual shutter was used to block exposure of the sample to the light. The sample was typically irradiated at an interval of 10 s.

2. 5 X-ray crystallography

The intensity data were collected on a Bruker APEX II diffractometer using graphite-monochromated Mo$K\alpha$ radiation (λ = 0.71073 Å) at room temperature. The structures were solved by direct methods and expanded using Fourier technique. The non-hydrogen atoms were refined with anisotropic thermal parameters, and hydrogen atoms were assigned with common isotropic displacement factors and included in the final refinement by using geometrical constraints. The structures were refined with full-matrix least-squares techniques on F^2 using the SHELXTL-97 program package[23, 24]. Crystal data: **1**: monoclinic, space group $C2/c$ with M_r = 1771.53, a = 24.5822(15), b = 13.0729(6), c = 16.1506(9) Å, β = 109.954(6) º, V = 4878.6(5) Å^3, Z = 4, D_c = 2.408 g/cm^3, F(000) = 3180, μ(Mo$K\alpha$) = 10.782 mm^{-1}, the final R = 0.0344, wR = 0.0941, S = 1.120, $(\Delta/\sigma)_{max}$ = 0.000, $(\Delta\rho)_{max}$ = 0.983 and $(\Delta\rho)_{min}$ = –2.116 e/Å^3. **2**: orthorhombic, space group $Pbca$ with M_r = 724.20, a = 22.636(3), b = 7.8012(12), c = 24.279(4) Å, V = 4287.3(11) Å^3, Z = 8, D_c = 2.244 g/cm^3, F(000) = 2672, μ(Mo$K\alpha$) = 13.535 mm^{-1}, the final R = 0.0379, wR = 0.0758, S = 1.053, $(\Delta/\sigma)_{max}$ = 0.000, $(\Delta\rho)_{max}$ = 0.948 and $(\Delta\rho)_{min}$ = –2.151 e/Å^3. Selected bond lengths and bond angles are given in Table 1, and C–H $\cdot\cdot\pi$ interactions are shown in Table 2.

Table 1. Selected Bond Lengths (Å) and Bond Angles (º)

	Bond	Dist.	Bond	Dist.	Bond	Dist.
	Pb(1)–I(1)^a	3.2174(7)	Pb(1)–I(1)	3.2174(7)	Pb(1)–I(2)^a	3.1422(9)
	Pb(1)–I(2)	3.1422(8)	Pb(1)–I(3)^a	3.3774(9)	Pb(1)–I(3)	3.3774(9)
	Pb(2)–I(1)^c	3.2289(7)	Pb(2)–I(1)	3.2289(7)	Pb(2)–I(2)^a	3.2193(7)
	Pb(2)–I(2)^b	3.2193(7)	Pb(2)–I(3)	3.2195(9)	Pb(2)–I(3)^c	3.2195(9)
1	Angle	(º)	Angle	(º)	Angle	(º)
	I(2)^a–Pb(1)–I(1)^a	92.31(2)	I(2)–Pb(1)–I(1)^a	88.25(2)	I(2)a–Pb(1)–I(1)	88.25(2)
	I(2)–Pb(1)–I(1)	92.31(2)	I(1)^a–Pb(1)–I(3)^a	82.21(2)	I(1)–Pb(1)–I(3)^a	97.36(2)
	I(1)^a–Pb(1)–I(3)	97.36(2)	I(1)–Pb(1)–I(3)	82.21(2)	I(1)^a–Pb(1)–I(1)	179.25(3)
	I(2)^a–Pb(2)–I(3)	83.65(2)	I(2)^b–Pb(2)–I(3)	96.35(2)	I(2)^a–Pb(2)–I(3)^c	96.35(2)
	I(2)^b–Pb(2)–I(3)c	83.65(2)	I(2)^a–Pb(2)–I(1)c	93.263(18)	I(2)^b–Pb(2)–I(1)^c	86.737(18)
	I(2)^a–Pb(2)–I(1)	86.737(18)	I(2)^b–Pb(2)–I(1)	93.263(18)	I(2)^a–Pb(2)–I(2)^b	180.00(2)
	Bond	Dist.	Bond	Dist.	Bond	Dist.
	Pb(1)–Br(1)	3.0356(11)	Pb(1)–Br(1)^b	3.0537(11)	Pb(1)–Br(2)	3.0321(10)
	Pb(1)–Br(2)^a	3.0508(10)	Pb(1)–Br(3)	3.0318(10)	Pb(1)–Br(3)^a	3.0558(10)
2	Angle	(º)	Angle	(º)	Angle	(º)
	Br(3)–Pb(1)–Br(1)	91.23(3)	Br(2)–Pb(1)–Br(1)	101.02(3)	Br(1)–Pb(1)–Br(2)^a	81.36(3)
	Br(2)–Pb(1)–Br(1)^b	81.37(3)	Br(2)^a–Pb(1)–Br(1)^b	103.06(3)	Br(1)–Pb(1)–Br(3)^a	84.55(3)
	Br(1)^b–Pb(1)–Br(3)^a	93.64(3)	Br(1)–Pb(1)–Br(1)^b	175.04(4)		

Symmetry codes for **1**: a –*x*, *y*, –*z* + 1/2; b: *x*, –*y*, *z*–1/2; c: –*x*, –*y*, –*z*; Symmetry codes for **2**: a: –*x* + 1/2, *y* – 1/2, *z*; b: –*x* + 1/2, *y* + 1/2, *z*

Table 2. C–H $\cdot\cdot\pi$ Interactions for 1 and 2

	C–H $\cdot\cdot\pi$	C $\cdot\cdot$ C$_g$/Å	H $\cdot\cdot$ C$_g$/Å	∠(C–H $\cdot\cdot$ C$_g$)/ º	Symmetry transformation
1	C(11)–H(11) $\cdot\cdot$ Cg(1)	3.783(14)	2.88	84	1/2–*x*, 1/2+*y*, 1/2–*z*
	C(17)–H(17) $\cdot\cdot$ Cg(2)	3.811(16)	2.88	70	*x*, –*y*, –1/2+*z*
	C$_g$(1): C(13)→C(14)→C(15)→C(16)→C(17)→C(18)→;				
	C$_g$(2): C(1)→C(2)→C(3)→C(4)→C(5)→C(6)→				
2	C(10)–H(10) $\cdot\cdot$ Cg(2)	3.796(12)	2.87	76	–*x*, 1/2+*y*, 1/2–*z*
	C$_g$(1): C(7)→C(8)→C(9)→C(10)→C(11)→C(12)→				

3 RESULTS AND DISCUSSION

3. 1 Description of the structures

Two hybrids are the combination of 1-*D* $(PbX_3)_n^{n-}$ (X = I and Br) polyanions and $(Ph_3PMe)^+$ template via electrostatic force. The $(PbX_3)_n^{n-}$ polyanion is the most common form in haloplumbates, in which Pb^{2+} centers are in octahedral environment[25]. The situation with three bridging halides can be described as a face-sharing mode, and the octahedra can share faces with either only *trans* fashion or alternated

trans/*cis* modes. The pure *trans* case gives long, straight chains whereas the latter case is wave-shaped with the amplitude perpendicular to the direction of the chain[26]. The $(PbX_3)_n^{n-}$ chain in this work can be divided into the former case, which is generated via *trans*-face sharing PbX_6 octahedra (Fig. 1). The PbI_6 octahedron in **1** is more distorted than $PbBr_6$ in **2** judged from the Pb–X distances and X–Pb–X angles (Table 1). The sizes of $(PbX_3)_n^{n-}$ nanochains are 0.43 and 0.41 nm for **1** and **2**, respectively. In $(Ph_3PMe)^+$ cations, the P atom in **1** is more distorted with tetrahedral angles of 108.82～111.75 ° (108.19～110.66 ° for **2**). In two hybrids, none of them exhibit C–H ··X hydrogen bonds, *π*-*π* interactions or anionic halogen-*π* interactions, and only C–H ··*π* interactions exist (Table 2). For $(Ph_3PMe)^+$ templates, C–H ··*π* interactions contribute to the formation of a 2-*D* wave-like layer in **1** and 1-*D* chain of **2** (Fig. 2). Finally, the $(PbX_3)_n^{n-}$ polyanions are surrounded by organic $(Ph_3PMe)^+$ templates via the C–H ··*π* interactions and electrostatic interactions (Fig. 3). Due to the presence of CH_3CN solvent in the lattice in **1**, its unit cell contains no residual solvent accessible void according to PLATON program. But the total potential solvent area of **2** is 56.3 Å^3, which hints more compact stacking in **1**.

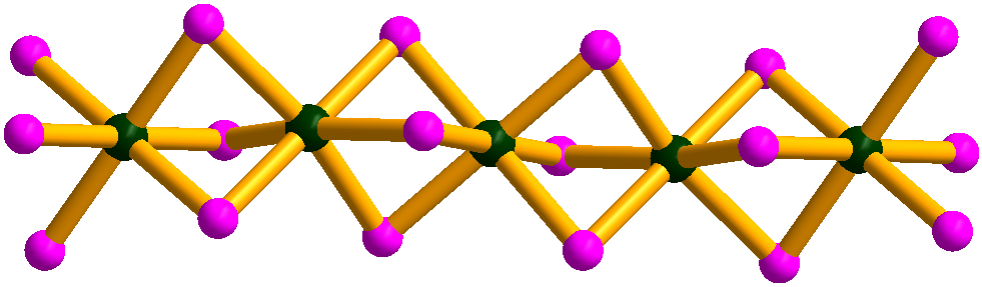

Fig. 1. 1-*D* $(PbX_3)_n^{n-}$ polyanions constructed from *trans* face-sharing PbX_6 octahedra

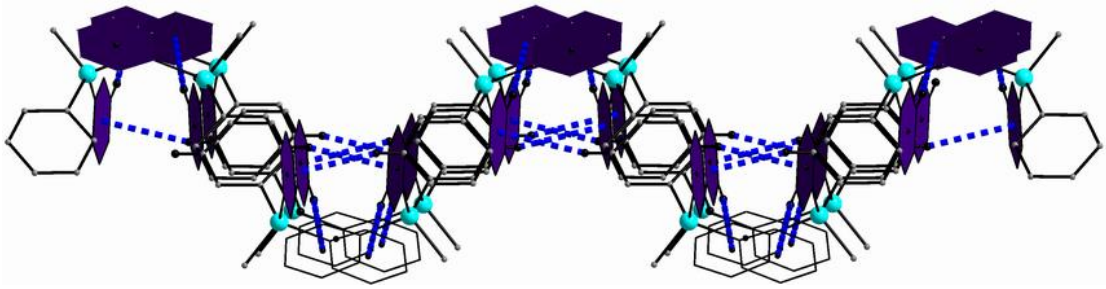

(a)

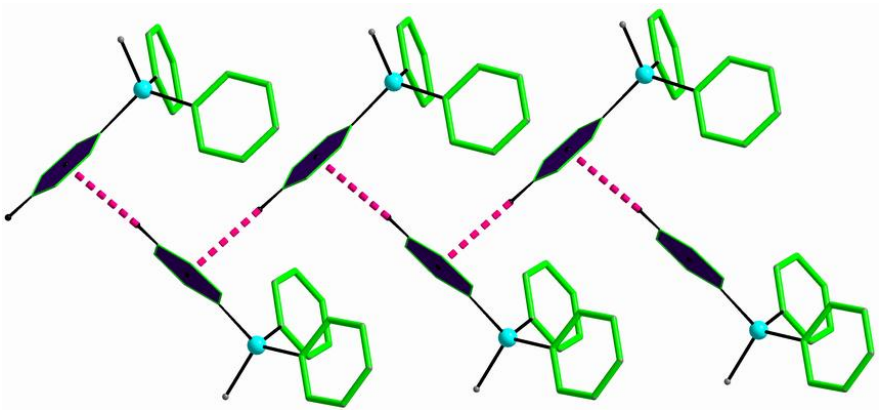

(b)

Fig. 2. (a) 2-*D* wave-like $(Ph_3PMe)_n^{n+}$ layer of 1 and (b) 1*D* $(Ph_3PMe)_n^{n+}$ chain in 2 based on C–H···*π* interactions (H atoms were omitted for clarity)

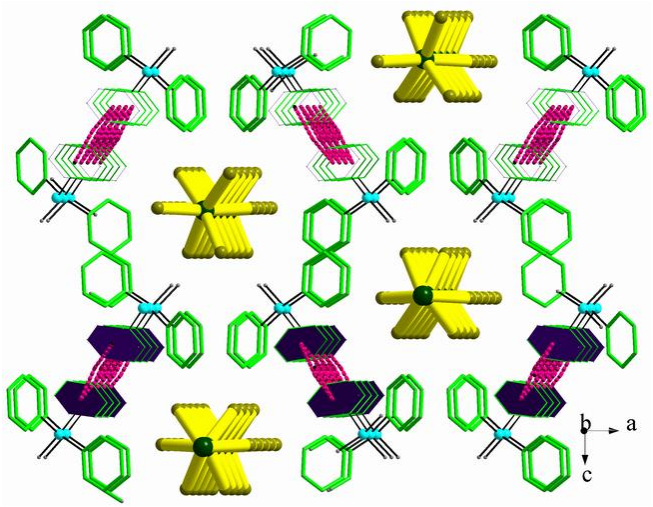

Fig. 3. Packing diagram showing the positions of 1-*D* $(PbX_3)_n^{n-}$ polyanions and organic templates

3. 2 Water stability studies

The phase purities of bulk compounds **1** and **2** have been verified by powder X-ray diffraction (PXRD). As shown in Fig. 4, the experimental patterns are consistent with the corresponding simulated ones, which suggest that the properties of as-synthesized samples can reflect their bulk performances. It is worth mentioning that one of the critical drawbacks of photoluminescence (PL) materials is their generally low water stability, which will deter their real applications[27]. During water stability study, the as-synthesized crystalline samples were ground as fine powders and soaked in deionized water at room temperature. Afterwards, the samples were centrifuged and dried at 40 ℃ at an interval of 2 days, then PXRD experiments were conducted again on the collected samples to check their phases. To our interest, two hybrids exhibit good water stabilities. In detail, **1** can maintain its structure after soaking in water for 5 day, but **2** will not collapse within 3 days. Their relatively good water stability can be assigned to the alkylation of PPh_3 as counteractions, in which both PPh_3 and methyl are typical hydrophobic species. Importantly, the absence of hydrogen bond donors on quaternary phosphorus salts can rule out the formation of typical strong hydrogen bonds with water in an aqueous system or in moist air, which improve their water stability[14]. The better water stability of **1** might be induced by its stronger C–H $\cdots\pi$ interactions, thus deterring the hydrolysis reaction.

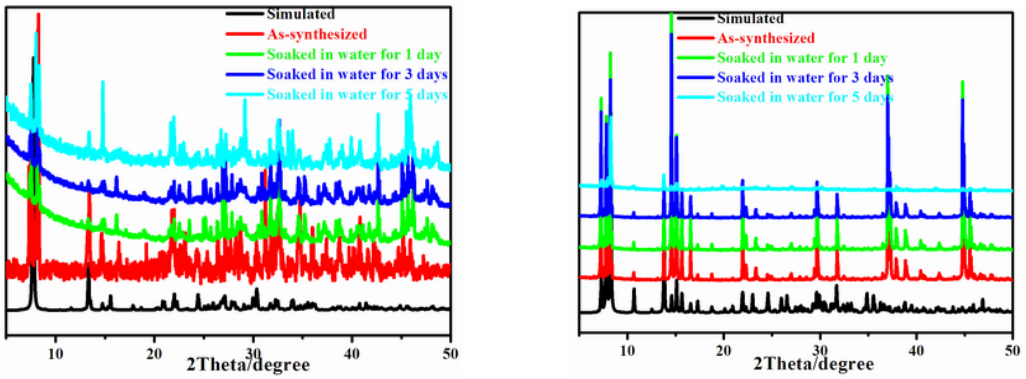

Fig. 4. PXRD patterns of 1 (a) and 2 (b) under different conditions

3. 3 Optical diffuse-reflection spectra

Solid-state optical diffuse-reflection spectra of **1**, **2** and $(Ph_3PMe)I$ template were recorded from powder samples at room temperature, which exhibit intense adsorption in ultraviolet zone (260 ～ 480 nm, Fig. 5). The organic $(Ph_3PMe)I$ absorbs at about 330 nm, corresponding to the n-π^*/π-π^* transitions of phenyl groups. After hybridization with haloplumbates, for **2**, the adsorption peaks change little,

which can be assigned to the more incompact stacking with weaker organic-inorganic interaction. But for **1**, the peaks shift to longer waves at about 390 nm. This might be induced by the stronger organic-inorganic interactions due to its more compact packing with the presence of lattice CH_3CN. Therefore, the corresponding electronic transitions of **1** and **2** can be ascribed to the ligand centered n-π^*/π-π^* transitions of phosphine cations[28]. The longer adsorption over 330 nm is relevant to ligand-to-ligand charge transfer (LLCT) between haloplumbates and organic cations[26, 29], which can be validated by their obvious ligand-to-ligand C–H $\cdots\pi$ interactions. The optical gaps of **1** and **2** have been deduced from UV-Vis diffuse-reflection spectra by the straightforward extrapolation method[30]. The gaps are about 2.71 and 3.44 eV, respectively, exhibiting obvious shifts compared with the measured value of bulk PbI_2 (2.47～2.49 eV)[31]. Clearly, the energy band gaps of this work mainly derive from the charge transfer of organic components, which is contrary to other haloplumbate/organic hybrids[32].

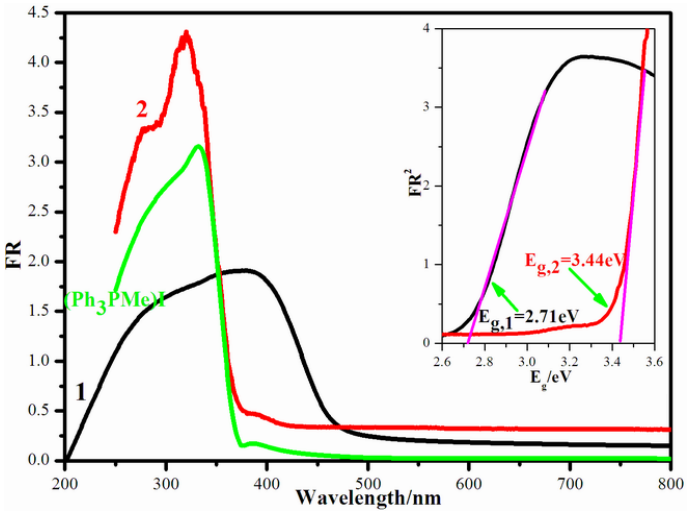

Fig. 5. Absorbance spectra of 1 and 2 (Inset: the band gaps calculated from *K-M* function)

3. 4 Photophysical properties

The room-temperature solid luminescence of **1** and **2** is shown in Fig. 6a. Two hybrids generate red emission in solid state at room temperature, emitting a single emission band with the maximum peaks at about 704 nm (λ_{ex} = 420 nm) for **1** and 651 nm (λ_{ex} = 330 nm) for **2**. Their luminescent colors are also shown by CIE-1931 emission profiles (Fig. 6b). It has been proved that the free organic quaternary phosphorus salts can exhibit strong emission band at around 485 nm[13, 14]. Therefore, the red emission in this work should stem from the electronic transitions within haloplumbates, in detail, the halide-to-metal charge transfer[26, 33]. Therefore, the emissions could be attributed to both free excitons and self-trapped excited states[34], because in the 1-*D* haloplumbate nanochains based on face-sharing octahedra, delocalized excitonic states can give rise to relatively weaker electron-phonon coupling, favoring the presence of both free excitons and self-trapped excitons[35]. The PLQEs of two hybrids are 5.89% and 5.93%, which are relatively lower compared to those of organic lead halide hybrids[34] perhaps due to the more nonradiative pathways in this nanochain structure.

The temperature-dependent emission property of **1** by measuring photoluminescence (PL) from 77 to 297 K was conducted to verify its luminescent thermochromic performance (Fig. 7). With the temperature cooled from 297 to 177 K, the emission intensity increases gradually, and the emission band changes little. But further cooling from 177 to 77 K will result in the decreased intensity. The emission band presents blue-shift firstly (about 680 nm at 157, 137 and 117 K) and then red-shift (736 nm for 97 K, 751 nm at 77 K, Fig. 7b). When the sample is gradually warmed up to room temperature, the red emission is back to the initial intensity, illustrating typical reversible luminescent thermochromic behavior. This phenomenon can be explained as follows: below 117 K, free and self-trapped excitons coexist because of a thermal activated equilibrium. As a result, blue-shift emissions can be produced. According to the structural analysis, haloplumbate nanochains are surrounded by organic cations to form the assembly of core-shell quantum well. Therefore, at temperature lower than 117 K, strong quantum

confinement will rule out the free excitons, and self-trapped excitons will dominate, thereby leading to red-shift luminescence[1, 36].

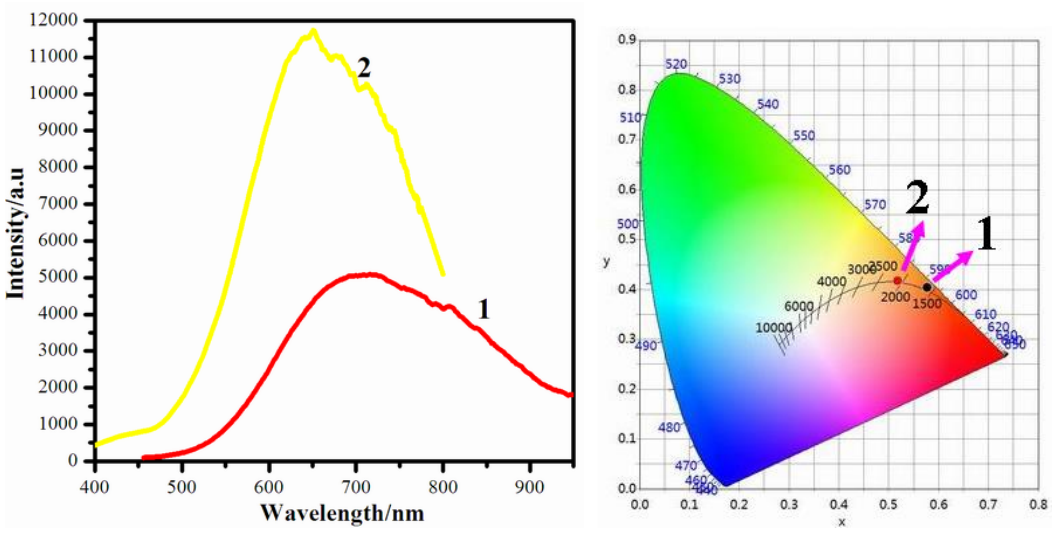

(a) **(b)**

Fig. 6. (a) Room temperature solid-state luminescence spectra and (b) CIE-1931 emission profiles of 1 and 2

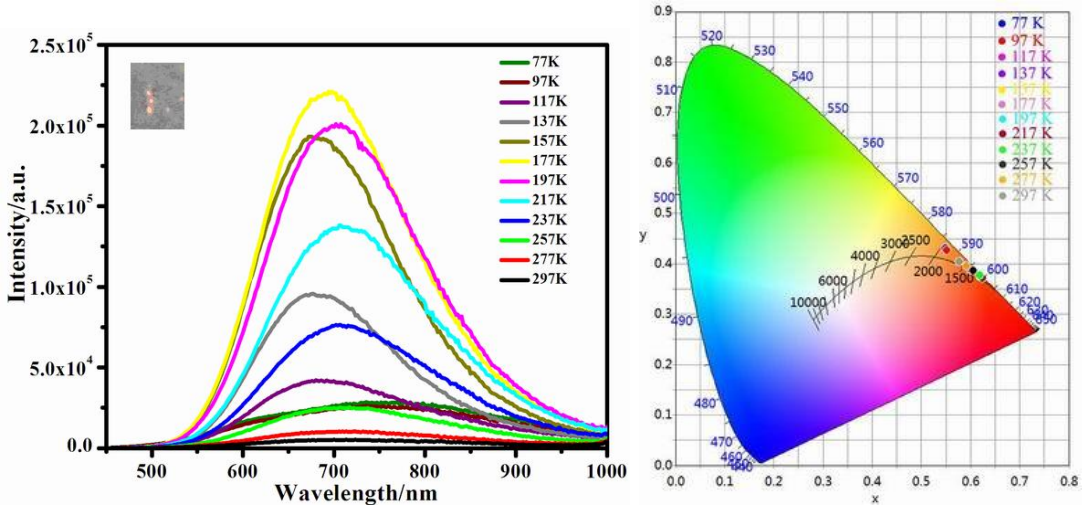

(a) **(b)**

Fig. 7. (a) Temperature-dependent PL spectra (excited at 420 nm, inserted: the photo at 77 K) and (b) CIE chromaticity coordinates of 1 from 77 to 297 K

3. 5 Photocurrent response performance

Photocurrent response is essential for new photo/electrical devices like photo-detection. Haloplumbate-based hybrids have demonstrated photocurrent response property[36]. In this work, photocurrent response measurements were conducted by typical three-electrode system according to literature method[37]. The photocurrent-time (*I*–*T*) curves of two samples in Na_2SO_4 aqueous solution under the illumination from a 150W Xe arc lamp with on-off cycles are shown in Fig. 7. To our interest, under the repetitive irradiation, repeatable photocurrents with rapid responses can be observed on two hybrids, and their photocurrents decrease firstly but stabilize after five cycles. The photocurrents are 0.06 and 0.18 μA/cm^2 for **1** and **2**, respectively. The current intensity of this work is weaker than that of other haloplumbate-based hybrids[36]. Besides, **2** has much higher current intensity than **1**, suggesting higher transferring efficiency of the photo-generated charge carriers on the **2**-coated film. The higher transferring efficiency should be induced by stronger inter-cation C–H $\cdots\pi$ interactions in **2**. According to universally accepted mechanism, the haloplumbate-Ph_3PMe^+ donor-acceptor systems are responsi-

ble for photocurrent generation (Fig. 7b): upon irradiation, the photosensitive Ph_3PMe^+ cations are excited to generate the $Ph_3PMe^{+\bullet}$ radicals; at the mean time, electron-rich $(PbX_3)_n^{n-}$ donors can transfer their electrons to Ph_3PMe^+ to form $(PbX_3)_n^{n-\bullet}$ radicals. Consequently, an electron conductive pair of $(PbX_3)_n^{n-\bullet}$–$Ph_3PMe^{+\bullet}$ can be constructed. Finally, all the radicals are transferred to the ITO electrode with re-production currents. Owing to the presence of CH_3CN solvent in **1**, some radicals are transferred to solvent and block the re-production current. As a result, a lower transferring efficiency will be given.

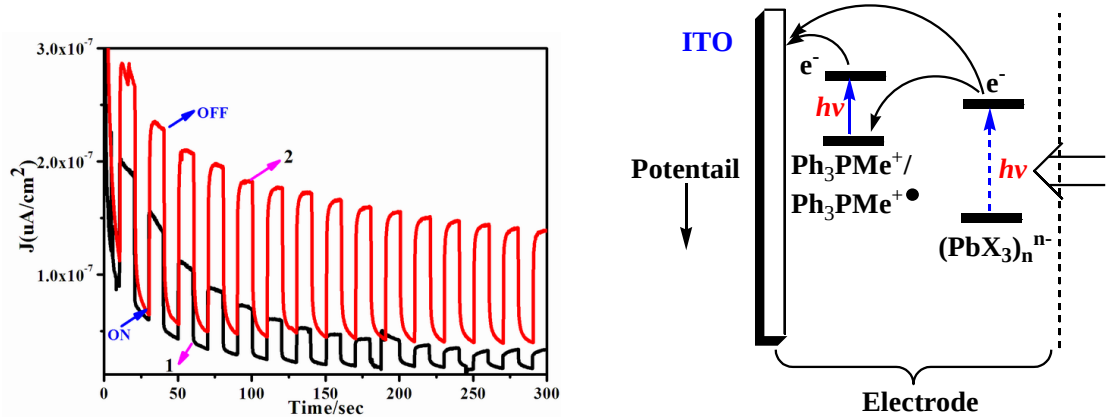

(a) **(b)**

Fig. 8. (a) Photocurrent response behaviors of 1 and 2; (b) Photocurrent response mechanism in this work

4 CONCLUSION

In summary, two triphenylmethylphosphonium/haloplumbate hybrids with core-shell quantum well have been prepared, in which the 1-*D* $(PbX_3)_n^{n-}$ nanochains are built from face-sharing PbX_6 octahedra. No other weak interactions expect C–H $\cdots\pi$ interaction can also be detected. Two hybrids exhibit good water stabilities. Interestingly, the adsorption performance mainly derives from the charge transfer of organic components, but their emissions stem exclusively from the inorganic $(PbX_3)_n^{n-}$ nanochains. At lower temperature, strong quantum confinement will rule out the free excitons, and self-trapped excitons will dominate, resulting in red-shift luminescence. Finally, effective and repeatable photocurrent responses can be detected in these hybrids. This work will be beneficial for the design of new multi-functional photo/electrical materials.

REFERENCES

(1) Wang, G. E.; Sun, C.; Wang, M. S.; Guo, G. C. Semiconducting crystalline inorganic-organic hybrid metal halide nanochains. *Nanoscale* **2020**, 12, 4771–4789.

(2) Zong, Y.; Wang, N.; Zhang, L.; Ju, M. G.; Zeng, X. C.; Sun, X. W.; Zhou, Y.; Padture, N. P. Homogenous alloys of formamidinium lead triiodide and cesium tin triiodide for efficient ideal-bandgap perovskite solar cells. *Angew. Chem. Int. Ed.* **2017**, 56, 12658−12662.

(3) Bekenstein, Y.; Koscher, B. A.; Eaton, S. W.; Yang, P.; Alivisatos, A. P. Highly luminescent colloidal nanoplates of perovskite cesium lead halide and their oriented assemblies. *J. Am. Chem. Soc.* **2015**, 137, 16008−16011.

(4) Wang, Y. K.; Wu, Y. L.; Lin, X. Y.; Wang, D. H.; Zhang, W. T.; Song, K. Y.; Li, H. H.; Chen, Z. R. Halobismuthate/diphenyliodonium hybrids stabilized by secondary hypervalent I(III) ⋯X interactions: structures, optical studies and thermochromisms. *J. Mole. Struct.* **2018**, 1151, 81−87.

(5) Peng, W.; Chen, Z. R.; Li, H. H. Tetrameric $(Bi_4I_{16})^{4-}$ iodobismuthate templated by 1,*ω*-bis(isoquinoline)alkane cation: structure, photoluminescence and enhanced thermochromism. *Chin. J. Struct. Chem.* **2019**, 38, 1485−1493.

(6) Wang, D. H.; Lin, X. Y.; Wang, Y. K.; Zhang, W. T.; Song, K. Y.; Lin, H.; Li, H. H.; Chen, Z. R. A new iodiplumbate-based hybird constructed from asymmetric viologen and polyiodides: structure, properties and photocatalytic activity for the degradation of organic dye. *Chin. J. Struct. Chem.* **2017**, 36, 2000−2006.

(7) Ramasamy, P.; Lim, D. H.; Kim, B.; Lee, S. H.; Lee, M. S.; Lee, J. S. All-inorganic cesium lead halide perovskite nanocrystals for photodetector applications. *Chem. Commun.* **2016**, 52, 2067−2070.

(8) Zeng, X. H.; He, X.; Chen, J. Y.; Zhang, J. W.; Li, H. H.; Chen, Z. R. Polymeric iodoplumbate templated by photochemically active coordination cation $[Ru(phen)_3]^{2+}$: structure and properties of a bimetallic inorganic-organic hybrid. *J. Clust. Sci*. **2014**, 25, 979–988.

(9) Wu, L. M.; Wu, X. T.; Chen, L. Structural overview and structure-property relationships of iodoplumbate and iodobismuthate. *Chem. Rev*. **2009**, 253, 2787−2804.

(10) Zhang, G.; Yin, J.; Song, X.; Fei, H. A moisture-stable organosulfonate-based metal-organic framework with intrinsic self-trapped white-light emission. *Chem. Commun.* **2020**, 56, 1325−1328.

(11) Lin, X. L.; Chen, B.; Huang, Y. R.; Song, K. Y.; Zhou, P. K.; Zong, L. L.; Li, H. H.; Chen, Z. R.; Rong, J. The achievement of intrinsic white-light-emitting by hybridization deformable haloplumbates with rigid luminescent naphthalene motif. *Inorg. Chem. Front.* **2020**, 7, 4477–4487.

(12) Sun, C.; Xu, G.; Jiang, X. M.; Wang, G. E.; Guo, P. Y.; Wang, M. S.; Guo, G. C. Design strategy for improving optical and electrical properties and stability of lead-halide semiconductors. *J. Am. Chem. Soc*. **2018**, 140, 2805–2811.

(13) Alam, P.; Leung, N. L. C.; Liu, J. K.; Cheung, T. S.; Zhang, X. P.; He, Z. K.; Kwok, R. T. K.; Lam, J. W. Y.; Sung, H. H. Y.; Williams, I. D.; Chan, C. C. S.; Wong, K. S.; Peng, Q.; Tang, B. Z. Two are better than one: a design principle for ultralong-persistent luminescence of pure organics. *Adv. Mater*. **2020**, 32, 2001026−7.

(14) Zhang, W. T.; Liu, J. Z.; Liu, J. B.; Song, K. Y.; Li, Y.; Chen, Z. R.; Li, H. H.; Jian, R. Quaternary phosphorus-induced iodocuprate(I)-based hybrids: water stabilities, tunable luminescences and photocurrent responses. *Eur. J. Inorg. Chem*. **2018**, 38, 4234–4244.

(15) Czado, W.; Muller, U. Tetraphenylphosphonium-trichloroplumbat(II), PPh_4PbCl_3 center dot CH_3CN. *Z. Anorg. Allg. Chem.* **1998**, 624, 925−926.

(16) Krautscheid, H.; Vielsack, F. Iodoplumbates with tetra- and penta-coordinated Pb^{2+} ions. *Z. Anorg. Allg. Chem*. **1999**, 625, 562−566.

(17) Krautscheid, H.; Lekieffre, J. F.; Besinger, J. Iodoplumbates with polymeric anions-synthesis and crystal structures of $[Na_3(OCMe_2)_{12}][Pb_4I_{11}(OCMe_2)]$, $(Ph_4P)_2[Pb_5I_{12}]$, and $(Ph_4P)_4[Pb_{15}I_{34}dmf_6]$. *Z. Anorg. Allg. Chem.* **1996**, 622, 1781−1787.

(18) Klapotke, T. M.; Krumm, B.; Polborn, K.; Rienacker, C. M. Synthesis and characterization of bromo- and bromochloroplumbates(II) crystal structures of $[Ph_4E]_2[Pb_3Br_8]$ (E = P, As) and $[Ph_4P][PbBrCl_2]CH_3CN$. *Z. Naturforsch. Teil B* **2000**, 55, 377−382.

(19) Elessawi, M.; Wartchow, R.; Berthold, H. J. Crystal structure of triphenylmethylphosphonium triiodoplumbate, $(P(C_6H_5)_3(CH_3))(PbI_3)$. *Z. Kristallogr.* **1997**, 212, 163−164.

(20) Zhao, Y.; Feng, T.; Li, G.; Liu, F.; Dai, X.; Dong, Z.; Qiu, X. Synthesis and properties of novel polyimide fibers containing phosphorus groups in the side chain (DATPPO). *RSC Adv*. **2016**, 6, 42482–42494.

(21) Lin, X. Y.; Zhao, L. M.; Wang, D. H.; Wang, Y. K.; Li, M.; Li, H. H.; Chen, Z. R. Structural diversities of squarate-based complexes: photocurrent responses and thermochromic behaviours enchanced by viologens. *Inorg. Chem. Front.* **2018**, 5, 189−199.

(22) Wang, D. H.; Zhao, L. M.; Lin, X. Y.; Wang, Y. K.; Zhang, W. T.; Song, K. Y.; Li, H. H.; Chen, Z. R. Iodoargentate/iodobismuthate-based materials hybridized with lanthanide-containing metalloviologens: thermochromic behaviors and photocurrent responses. *Inorg. Chem. Front.* **2018**, 5, 1162–1173.

(23) Sheldrick, G. M. *SHELXS 97, Program for the Solution of Crystal Structures.* University of Götingen, Germany **1997**.

(24) Sheldrick, G. M. *SHELXL 97, Program for the Refinement of Crystal Structures.* University of Göttingen, Germany **1997**.

(25) Li, H. H.; Wang, Y. J.; Lian, Z. X.; Xu, Y. F.; Wang, M.; Huang, S. W.; Chen, Z. R. An additional structure and property study on polymeric haloplumbates(II) with aromatic N-heterocyclic organic molecules. *J. Mole. Struct.* **2012**, 1016, 118−125.

(26) Krautscheid, H.; Lode, C.; Vielsack, F.; Vollmer, H. Synthesis and crystal structures of iodoplumbate chains, ribbons and rods with new structural types. *J. Chem. Soc. Dalton Trans.* **2001**, 7, 1099−1104.

(27) Liu, W.; Zhu, K.; Teat, S. J.; Dey, G.; Shen, Z. Q.; Wang, L.; O'Carroll, D. M.; Li, J. All-in-one: achieving robust, strongly luminescent and highly dispersible hybrid materials by combining ionic and coordinate bonds in molecular crystals. *J. Am. Chem. Soc*. **2017**, 139, 9281–9290.

(28) Huang, C. H.; Wen, M.; Wang, C. Y.; Lu, Y. F.; Huang, X. H.; Li, H. H.; Wu, S. T.; Zhuang, N. F.; Hu, X. L. A series of pure-blue-light emitting Cu(I) complexes with thermally activated delayed fluorescence: structural, photophysical, and computational studies. *Dalton Trans*. **2017**, 46, 1413–1419.

(29) Xu, L. J.; Wang, J. Y.; Zhu, X. F.; Zeng, X. C.; Chen, Z. N. Phosphorescent cationic Au_4Ag_2 alkynyl cluster complexes for efficient solution-processed organic light-emitting diodes. *Adv. Funct. Mater*. **2015**, 25, 3033–3042.

(30) Schevciw, O.; White, W. B. The optical absorption edge of rare earth sesquisulfides and alkaline earth-rare earth sulfides. *Mater. Res. Bull*. **1983**, 18, 1059−1062.

(31) Baibarac, M.; Preda, N.; Mihut, L.; Baltog, I.; Lefrant, S.; Mevellec, J. Y. On the optical properties of micro-and nanometric size PbI_2 particles. *J. Phys. Condens. Mat.* **2004**, 16, 2345−2356.

(32) Liu, B.; Xu, L.; Guo, G. C.; Huang, J. S. Three inorganic-organic hybrids of bismuth(III) iodide complexes containing substituted 1,2,4-triazole organic components with characterization of diffuse reflectance spectra. *J. Solid State Chem*. **2006**, 179, 1611−1617.

(33) Zhang, Z. J.; Xiang, S. C.; Zhang, Y. F.; Wu, A. Q.; Cai, L. Z.; Guo, G. C.; Huang, J. S. A new type of hybrid magnetic semiconductor based upon polymeric iodoplumbate and metal-organic complexes as templates. *Inorg. Chem*. **2006**, 45, 1972−1977.

(34) Yuan, Z.; Zhou, C.; Shu, Y.; Tian, Y.; Messier, J.; Wang, J.; Burgt, L.; Kountouriotis, K.; Xin, Y.; Holt, E.; Schanze, K. S.; Clark, R.; Siegrist, T.; Ma, B. One-dimensional organic lead halide perovskites with efficient bluish white-light emission. *Nat. Commun.* **2017**, 8, 14051−7.

(35) Lin, H.; Zhou, C. K.; Tian Y.; Besara, T.; Neu, J.; Siegrist, T.; Zhou, Y.; Bullock, J.; Schanze, K. S.; Ming, W. M.; Du, M. H.; Ma, B. W. Bulk assembly of organic metal halide nanotubes. *Chem. Sci*. **2017**, 8, 8400–8404.

(36) He, Y.; Huang, Y. R.; Li, Y. L.; Li, H. H.; Chen, Z. R.; Jiang, R. Encapsulating halometallates into 3-*D* lanthanide-viologen frameworks: controllable emissions, reversible thermochromism, photocurrent responses and electrical bistability behaviors. *Inorg. Chem.* **2019**, 58, 13862−13880.

(37) Sun, Y. G.; Ji, S. F.; Huo, P.; Yin, J. X.; Huang, Y. D.; Zhu, Q. Y.; Dai, J. Role of the coordination center in photocurrent behavior of a tetrathiafulvalene and metal complex dyad. *Inorg. Chem.* **2014**, 53, 3078–3087.